

Nanoscale

Accepted Manuscript



This is an *Accepted Manuscript*, which has been through the Royal Society of Chemistry peer review process and has been accepted for publication.

Accepted Manuscripts are published online shortly after acceptance, before technical editing, formatting and proof reading. Using this free service, authors can make their results available to the community, in citable form, before we publish the edited article. We will replace this *Accepted Manuscript* with the edited and formatted *Advance Article* as soon as it is available.

You can find more information about *Accepted Manuscripts* in the [Information for Authors](#).

Please note that technical editing may introduce minor changes to the text and/or graphics, which may alter content. The journal's standard [Terms & Conditions](#) and the [Ethical guidelines](#) still apply. In no event shall the Royal Society of Chemistry be held responsible for any errors or omissions in this *Accepted Manuscript* or any consequences arising from the use of any information it contains.

COMMUNICATION

Lanthanide-doped NaGdF₄ core-shell nanoparticles for non-contact self-referencing temperature sensors

Cite this: DOI: 10.1039/x0xx00000x

Shuhong Zheng,^a Weibo Chen,^a Dezhi Tan,^a Jiajia Zhou,^b Qiangbing Guo,^a Wei Jiang,^a Cheng Xu,^a Xiaofeng Liu*^{a,c} and Jianrong Qiu*^{a,c}

DOI: 10.1039/x0xx00000x

www.rsc.org/

We report that non-contact self-referencing temperature sensors can be realized with the use of core-shell nanostructure. These lanthanide-based nanothermometers (NaGdF₄:Yb³⁺/Tm³⁺@Tb³⁺/Eu³⁺) exhibit higher sensitivity at a wide range from 125 to 300 K based on two emissions of Tb³⁺ at 545 nm and Eu³⁺ at 615 nm under the near-infrared laser excitation.

Lanthanide ions (Ln³⁺)-activated nanomaterials have been intensively explored as nanothermometers (NTMs) that can be used as optical thermal probes in various fields.¹ In these emissive thermal probes, temperature determination is based on the strong dependence of the emission characteristics, such as emission energy, intensity and lifetime, on the temperature of the surrounding environment.^{1a} These luminescent NTMs which feature high-spatial resolution, fast response, noninvasive operation, are regarded as the most versatile and promising thermal probes working at the nanoscale environment.² Furthermore, by referring temperature to intensity ratios of selected dual emission bands rather than an individual emission peaks, it becomes possible to avoid common drawbacks found for conventional thermometers whose accuracy is largely affected by the sensor's concentration, excitation power, the drifts of the optoelectronic system and the computational treatment based on a single-transition intensity.³

There have been some recent examples in which Ln³⁺-based NTMs served as self-referencing nanoscale probes for thermographic applications in biological systems. Particularly, based on an up-conversion (UC) mechanism in certain Ln³⁺-ion couples, visible emission can be effectively generated under near infrared (NIR) irradiation, which therefore is highly suitable for biological application because of its deeper tissue penetration and less damage as compared to ultraviolet excitation.⁴ For instance, in Er³⁺/Yb³⁺ co-doped NaYF₄,⁵ Tm³⁺/Yb³⁺ co-doped CaF₂,⁶ and Nd³⁺ doped NaYF₄ nanoparticles (NPs),⁷ the temperature of the studied biological systems can be evaluated based on the ratio of the UC emission intensity from different thermally populated 4f levels (i.e., ²H_{11/2} and ⁴S_{3/2} level for Er³⁺) as well as from adjacent sub-Stark levels (i.e., two Stark components of the ⁴F_{3/2} multiplet of the Nd³⁺ ions). However, all of these NTMs still suffer the common inherent drawbacks of a low temperature resolution (for Nd³⁺ ~0.1% K⁻¹ and

for Tm³⁺ ~0.25% K⁻¹). This is partly due to the fact that the monitored emissions in the above systems come from two adjacent bands of the same ion which exhibit similar temperature dependence. Practical applications are therefore seriously jeopardized as an accurate and complicated computational system may be required.

Ratiometric self-referencing temperature determination based on emission bands from different ions rather than a single ion are therefore much preferred, which has been demonstrated with e.g. Eu³⁺-Tb³⁺ codoped metal organic frameworks (MOFs) and a higher sensitivity was achieved.⁸ Since these MOFs are not penetrable to tissue cells and only UV excitable, they are still not ideal for application, especially in biological fields.^{1b,9}

In order to solve these issues, we design here a self-referencing NIR-excitable NTM (shown in Fig.1) based on lanthanide-doped core-shell nanostructure. The core/shell structure allow flexible design and the facile incorporation of dopants with desired special distribution, allowing the manipulation of energy transfer among different ions.¹⁰ In this report, hexagonal-phase NaGdF₄ was chosen as the host material as it is easy to render high UC efficiency, produce relatively small and uniform NPs¹¹ and to tailor its surface chemistry for specific applications.^{4a,9a} Yb³⁺/Tm³⁺ couple was doped in the core which harvest NIR photons and then promote Gd³⁺ in the shell to the excited state through a two-step energy transfer (ET) via Yb³⁺-Tm³⁺-Gd³⁺.^{11b,c} Tb³⁺/Eu³⁺ couple (or i-Re³⁺) was chosen as the dopant in the shell. Due to ET from Gd³⁺ to Tb³⁺, Eu³⁺, strong visible green emission from Tb³⁺ (~545 nm) and red emission from Eu³⁺ (~615 nm) are resulted^{11b,12} and their luminescent intensities are

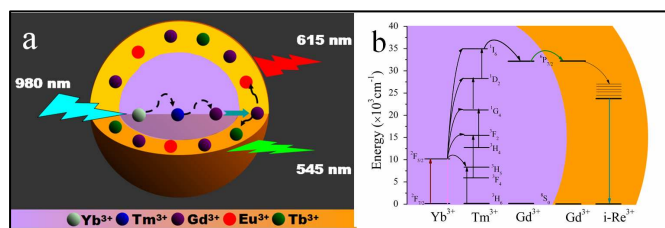


Fig.1 (a) Schematic design of Lanthanide-doped NaGdF₄@NaGdF₄ core-shell nanoparticle for NTMs; (b) The energy levels of the Ln³⁺-ions and energy transfer mechanisms in the core-shell nanoparticles.

temperature-dependent. Using a ratiometric measurement, we demonstrate that a sensitivity of 1.2% per K can be attained in a broader temperature range of 125 to 300 K based on the two emission bands of Tb^{3+} centered at 545 nm and Eu^{3+} at 615 nm. These results are attractive for precise temperature sensing under the NIR irradiation in practical applications.^{9b}

The hexagonal-phase NPs of $\text{NaGdF}_4:0.5 \text{ mol } \% \text{ Tm}^{3+}/49 \text{ mol } \% \text{ Yb}^{3+}$, core-shell $\text{NaGdF}_4:0.5 \text{ mol } \% \text{ Tm}^{3+}/49 \text{ mol } \% \text{ Yb}^{3+}@\text{NaGdF}_4:15 \text{ mol } \% \text{ Tb}^{3+}$, $\text{NaGdF}_4:0.5 \text{ mol } \% \text{ Tm}^{3+}/49 \text{ mol } \% \text{ Yb}^{3+}@\text{NaGdF}_4:1.5 \text{ mol } \% \text{ Eu}^{3+}$ and $\text{NaGdF}_4:0.5 \text{ mol } \% \text{ Tm}^{3+}/49 \text{ mol } \% \text{ Yb}^{3+}@\text{NaGdF}_4:15 \text{ mol } \% \text{ Tb}^{3+}/1.5 \text{ mol } \% \text{ Eu}^{3+}$ (donated as TY, TY@Tb, TY@Eu and TY@Tb/Eu, respectively) were synthesized via a thermal-decomposition route described previously in the literature.^{11c} Powder X-ray diffraction (XRD) analysis was carried out on a D/MAX-2550pc diffractometer with $\text{Cu K}\alpha$ ($\lambda=0.15418 \text{ nm}$) radiation at room temperature. Transmission electron microscopy (TEM) was performed using a FEG-TEM (Tecnai G2 F30 S-Twin, Philips-FEI, Netherlands). Temperature-dependent emission spectra and luminescence decay curves were recorded by a FLS920 fluorescence spectrophotometer (Edinburgh Instrument Ltd, UK) with a 1 W 980 nm laser diode. All the optical measurements were carried out under the same experimental configuration; only the sample temperature was changed to study the temperature dependence of UC intensity.

Fig. 2a shows the XRD patterns of the as-synthesized TY core and TY@Tb/Eu core-shell NPs. The strongest four diffraction peaks can be unambiguously indexed to the diffractions of the hexagonal-phase NaGdF_4 (JPCDS.No.27-0699). From the TEM images, the as-synthesized TY NPs were spherical, nearly monodisperse (Fig. 2b) and highly crystalline, which is also clearly indicated by the corresponding high-resolution TEM (HRTEM) image (Fig. 2c). The lattice fringes are clearly resolved, and a typical d-spacing around 0.52 nm is observed, corresponding to the (100) plane of hexagonal-phase NaGdF_4 . The increase of average particles size from $\sim 13 \text{ nm}$ to $\sim 25 \text{ nm}$ (Fig. 2d-e) suggests that the epitaxial shell has a thickness of around 12 nm.

Since all samples have the same core doped with the same concentration of Yb^{3+} and Tm^{3+} ions, the luminescence spectra are normalized with respect to the emission of Tm^{3+} at 650 nm for further analysis (Fig. 3a and b). Under NIR excitation at 980 nm, emission peaks at $\sim 290 \text{ nm}$ ($\text{Tm}^{3+}:^1\text{I}_6\text{-}^3\text{H}_6$) and $\sim 311 \text{ nm}$ ($\text{Gd}^{3+}:^6\text{P}_{7/2}\text{-}^8\text{S}_{7/2}$) were observed in addition to the visible emissions (Fig. 3a), which indicates that an ET process from Tm^{3+} to Gd^{3+} occurs efficiently because there is a large energy level overlap between $\text{Tm}^{3+}:^1\text{I}_6$ and $\text{Gd}^{3+}:^6\text{P}_{7/2}$.^{11b}

Fig. 3b shows the UC emission spectra for all samples from 500 nm to 630 nm. Upon NIR excitation at 980 nm, the TY (core only) NPs exhibit no emission peaks. In stark contrast, the UC emission spectrum for the core-shell NPs differs markedly from that of the original core NPs after coating an extra shell doped singly with Tb^{3+} , Eu^{3+} or with $\text{Tb}^{3+}/\text{Eu}^{3+}$ couple. A set of new UC emission peaks in the visible range can be unambiguously assigned to the characteristic transitions of Eu^{3+} and Tb^{3+} in the shell, instead of Tm^{3+} in the core.¹² These strong Tb^{3+} and Eu^{3+} emission peaks (also shown in Fig. 3c) can be rationalized considering two factors. First, trivalent Gd^{3+} ions can serve as a second sensitizer, which absorbs the energy from Tm^{3+} and subsequently transfer energy to the neighboring Tb^{3+} and Eu^{3+} ions (as shown in Fig. 1).^{11b,13} Second, the backward ET from $i\text{-Re}^{3+}$ ($i\text{-Re}^{3+}=\text{Tb}^{3+}, \text{Eu}^{3+}$) and Tm^{3+} which may quench the emission of $i\text{-Re}^{3+}$ as reported in previous work,^{11c} could be significantly minimized due to the core-shell configuration in the present case. It has to be further noted here that, benefited from the low phonon energy of host materials, the fine structures of the

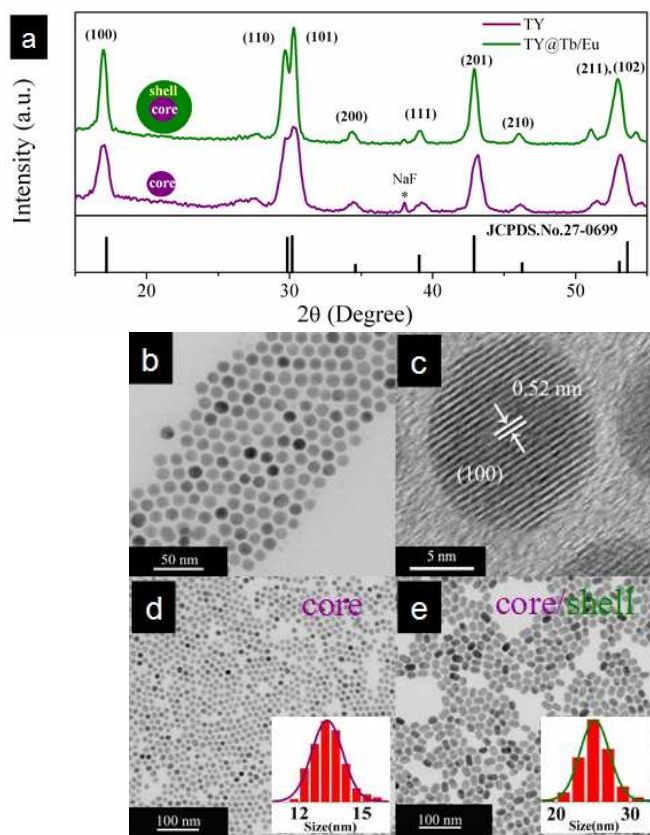


Fig. 2 (a) X-ray diffraction patterns of $\text{NaGdF}_4:\text{Tm}^{3+}/\text{Yb}^{3+}$ (0.5/49%) core only (marked with TY, purple line) nanoparticles and the corresponding core-shell nanoparticles coated with $\text{NaGdF}_4:\text{Tb}^{3+}/\text{Eu}^{3+}$ (15/1.5%) shell (marked with TY@Tb/Eu, green line). The standard pattern of NaGdF_4 (JPCDS No.27-0699) is provided as a reference. (b) and (c) Low and High-resolution TEM images of the as-synthesized $\text{NaGdF}_4:\text{Tm}^{3+}/\text{Yb}^{3+}$ (0.5/49%) nanoparticles. (d) and (e) TEM images of $\text{NaGdF}_4:\text{Tm}^{3+}/\text{Yb}^{3+}$ (0.5/49%) nanoparticles and the corresponding core-shell nanoparticles coated with a $\text{NaGdF}_4:\text{Tb}^{3+}/\text{Eu}^{3+}$ (15/1.5%) shell, respectively, the corresponding size distributions are also showed, respectively.

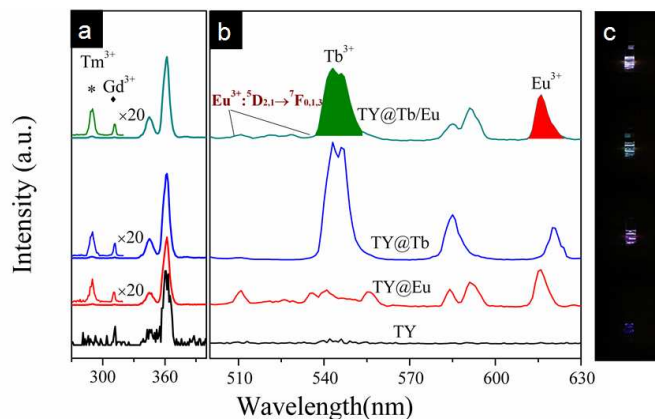


Fig. 3 (a) and (b) Upconversion emission spectra of the as-prepared core or core-shell nanoparticles doped with different Lanthanide ions in different wavelength ranges. (c) Photographs of corresponding samples in cyclohexane solution (2 mg mL^{-1}) under a 980 nm laser irradiation.

emission peaks of Eu^{3+} from ~ 510 to ~ 550 nm corresponding to ${}^5\text{D}_2$ - ${}^7\text{F}_3$ and ${}^5\text{D}_1$ - ${}^7\text{F}_1$ ($J=0,1$) can also be clearly detected.¹³ More importantly, compared to the singly doped NPs (blue and red line in Fig.3b), in the co-doped sample TY@Tb/Eu the emission intensity from Tb^{3+} : ${}^5\text{D}_4$ - ${}^7\text{F}_2$ (~ 545 nm) decreases remarkably whereas the emission from Eu^{3+} : ${}^5\text{D}_0$ - ${}^7\text{F}_2$ (~ 615 nm) seems unchanged (marked with the green and red area in Fig.3b). This result suggests that a possible ET between Tb^{3+} and Eu^{3+} ions may occur in the shell.

To verify the possible interactions between Tb^{3+} and Eu^{3+} ions, the decay curves of different emission bands for each sample were measured. The fluorescence lifetimes were also calculated as shown in Fig.4a (inset table). It is worth noting that the decay curves and lifetimes corresponding to the relative energy levels exhibit an evident change after doping Tb^{3+} and Eu^{3+} ions into the shell. For Eu^{3+} ions, the lifetime of the emission from ${}^5\text{D}_2$ state becomes significant shorter and those of ${}^5\text{D}_1$, ${}^5\text{D}_0$ states become longer in the TY@Tb/Eu NPs than those of the value obtained for the singly doped TY@Eu NPs. Meanwhile, a shorter lifetime for the emission from ${}^5\text{D}_4$ (Tb^{3+} ions) state is recorded after co-doping for the TY@Tb/Eu NPs compared to the TY@Tb NPs, suggesting again the presence of significant energy transfer between Tb^{3+} and Eu^{3+} in the shell (shown in Fig.4b).

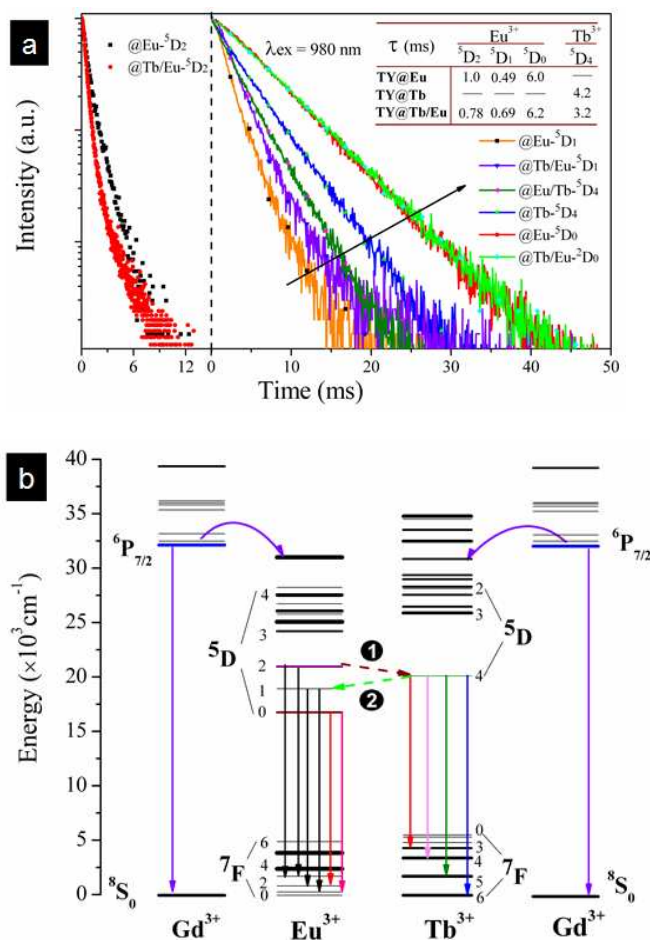


Fig.4 (a) Decay curves of Eu^{3+} (${}^5\text{D}_2$, ${}^5\text{D}_1$ and ${}^5\text{D}_0$) and Tb^{3+} (${}^5\text{D}_4$) in singly doped and codoped NaGdF_4 -base core-shell nanoparticles by excitation at 980 nm. The inset table lists the radiative lifetimes for different transitions of different samples. (b) Energy level diagrams of Gd^{3+} , Tb^{3+} , Eu^{3+} , and the proposed energy transfer and phonon-assisted process.

Based on the interaction between Tb^{3+} and Eu^{3+} illustrated above, the photoluminescence (PL) of Ln^{3+} ions may show a temperature-dependent behavior as revealed by previous works.^{2a, 8} Inspired by these observations, we suggest that the TY@Tb/Eu NPs might be used as self-referencing ratiometric NTMs based on the temperature dependence of the intensity ratio of green and red emission.

To examine the thermal effect on the PL behavior, the PL intensity was recorded at temperatures ranging from 50 to 300 K under excitation at 980 nm. The UC intensities of both Tb^{3+} and Eu^{3+} ions show obvious decrease with the rise in sample temperature. However, it's interesting that the intensity of Tb^{3+} (~ 545 nm) exhibits a significantly different temperature-dependent luminescent behavior as compared to that of the Eu^{3+} (~ 615 nm) (Fig.5a). The emission intensity of 545 nm (Tb^{3+}) shows linear temperature dependence whereas the 615 nm (Eu^{3+}) emission are much less affected by the changing of temperature. Therefore, in this work the emission intensity ratio of the ${}^5\text{D}_4$ - ${}^7\text{F}_5$ (Tb^{3+} at 545 nm) to ${}^5\text{D}_0$ - ${}^7\text{F}_2$ (Eu^{3+} at 615 nm) transition (donated as $I_{\text{Tb}}/I_{\text{Eu}}$) is used as a self-calibrated reference for the sample temperature, such that the well-known drawbacks of intensity-based measurements (e.g., variation with the sensor concentration) can be easily circumvented. From 125

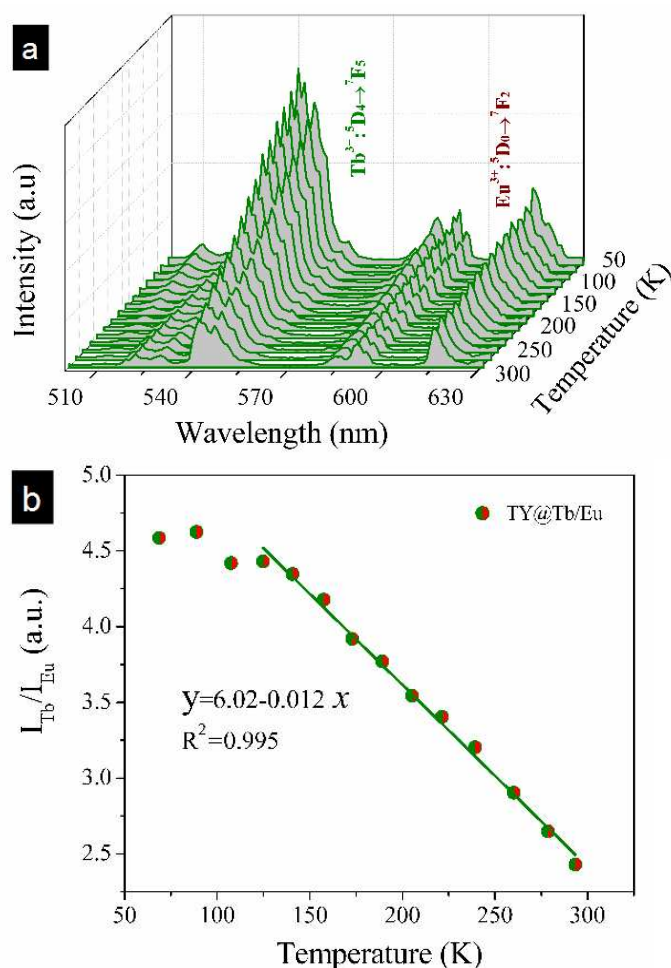


Fig.5 (a) Upconversion emission spectra of $\text{NaGdF}_4:\text{Tm}^{3+}/\text{Yb}^{3+}(0.5/49\%)@ \text{NaGdF}_4:\text{Tb}^{3+}/\text{Eu}^{3+}(15/1.5\%)$ core-shell nanoparticles recorded between 50 and 300 K. (b) Temperature-dependence of intensity ratio of Tb^{3+} (~ 545 nm) to Eu^{3+} (~ 615 nm) and the linear fitting curve for $\text{NaGdF}_4:\text{Tm}^{3+}/\text{Yb}^{3+}(0.5/49\%)@ \text{NaGdF}_4:\text{Tb}^{3+}/\text{Eu}^{3+}(15/1.5\%)$ core-shell nanoparticles.

to 300 K the following linear dependence of $I_{\text{Tb}}/I_{\text{Eu}}$ on temperature is found for the TY@Tb/Eu:

$$I_{\text{Tb}}/I_{\text{Eu}} = 6.02 - 0.012T \quad (1)$$

This result suggests that TY@Tb/Eu is an excellent luminescent thermometer in this temperature range under the NIR irradiation. As shown in Fig.5b, the sensitivity of this new NTMs is about 1.2% per K, which is a relative high value for inorganic materials.¹⁴ It is worthy stressing here that due to the sufficient strong emission intensity, and large energy gap between Tb^{3+} and Eu^{3+} , the temperature-dependent PL in the TY@Tb/Eu is much easier to detect, thus making them excellent candidate for non-contact self-referencing luminescent NTMs.

The final discussion concerns the reasons contributing to the distinct temperature dependence of Tb^{3+} and Eu^{3+} in the temperature range of 50 to 300 K. In general, an increment in the temperature leads to faster non-radiative transition through different pathways, such as phonon-assisted transitions and cross-relaxations between nearby ions.^{1a,15} For both of the Tb^{3+} and Eu^{3+} singly doped NPs, however, the energy gap between the emission level and the lower levels are too large to be bridged by phonons that can be provided by the host matrix ($\sim 350 \text{ cm}^{-1}$ for NaGdF₄), thus resulting in negligible phonon-assisted transitions (refer to Fig.S1 and Fig.S2 in electronic supplementary information).^{15,16b} For the codoped samples, in contrast, the non-radiative rate from the $\text{Tb}^{3+} {}^5\text{D}_4$ state can be drastically increased in the presence of nearby Eu^{3+} ions. This non-radiative de-excitation probability of the $\text{Tb}^{3+} {}^5\text{D}_4$ state ($\sim 20500 \text{ cm}^{-1}$) can be approximately described by the Mott-Seitz model¹⁶ by eq.2

$$K_{\text{nr}} \propto \exp\left(-\frac{\Delta E}{\kappa_{\text{B}}T}\right) \quad (2)$$

Where K_{nr} is the non-radiative probability, ΔE is the energy gap between the ${}^5\text{D}_4$ state and the lower level, κ_{B} is the Boltzmann constant and T is the absolute temperature. As the ${}^5\text{D}_4$ state ($\sim 20500 \text{ cm}^{-1}$) of Tb^{3+} is located near the center of ${}^5\text{D}_2$ ($\sim 21500 \text{ cm}^{-1}$) and ${}^5\text{D}_1$ ($\sim 19000 \text{ cm}^{-1}$) state of Eu^{3+} , the energy mismatch (ΔE) in this excited states of Tb^{3+} and Eu^{3+} are much closer to the maximal phonon energy of the host, resulting in a strong interaction between Tb^{3+} and Eu^{3+} , as confirmed by the lifetime measurement. This mechanism is elucidated schematically in Fig.4b. With the participation of several photons, this multi-phonon-assisted energy transfer from Tb^{3+} to Eu^{3+} ions becomes stronger in codoped samples and increases rapidly with temperature (T).^{16b,17} Consequently, the intensity of ${}^5\text{D}_4 \rightarrow {}^7\text{F}_2$ (Tb^{3+} at 545 nm) drops dramatically with the increase in temperature, giving higher sensitivity to temperature change.

In summary, we designed a new strategy based on core-shell nanostructure for ratiometric optical NTMs under NIR irradiation. Through controlling the types of Ln^{3+} dopant ions in NaGdF₄ NPs, the NIR energy can be effectively absorbed, up-converted, migrated and finally results in sufficiently strong temperature-dependent green and red emission, allowing the demonstration of an efficient NTM. Particularly, there are some unique features of TY@Tb/Eu as NTMs. Firstly, the large difference in energy between the emission of Tb^{3+} and Eu^{3+} makes the spectra easier to be detected and calculated based on relative intensity measurement compared to single-ion based systems. Secondly, their small size and adjustable surface chemistry endow them high performance in nanoscale environment with good spatial and temperature resolution.

This work was financially supported by the National Natural Science Foundation of China (Grant Nos. 51132004 and 51102209), the National Basic Research Program of China (2011CB808100),

and the Program for Changjiang Scholars and Innovative Research Team in University.

Notes and references

^a State Key Laboratory of Silicon Materials, Department of Materials Science and Engineering, Zhejiang University, Hangzhou, Zhejiang, 310027, P. R. China. E-mail:qjr@zju.edu.cn; Fax: +86 57188925079; Tel: +86 57188925079.

^b College of Materials Science and Engineering, China Jiliang University, Hangzhou, Zhejiang, 310018, P. R. China.

^c State Key Laboratory of Luminescent Materials and Devices, South China University of Technology, Guangzhou, Guangdong, 510640, P. R. China.

† Electronic supplementary information (ESI) available: Experimental details and supplementary data. See DOI: 10.1039/c000000x/

- a) D. Jaque and F. Vetrone, *Nanoscale*, 2012, **4**, 4301; b) X. J. Xue, F. Wang and X. G. Liu, *J. Mater. Chem.*, 2011, **21**, 13107; c) X.-D. Wang, O. S. Wolfbeis and R. J. Meier, *Chem. Soc. Rev.*, 2013, **42**, 7834; d) C. D. S. Brites, P. P. Lima, N. J. O. Silva, A. Millán and V. S. Amaral, *Nanoscale*, 2012, **4**, 4799.
- a) A. Cadiou, C. D. S. Brites, P. M. F. J. Costa, R. A. S. Ferreira, J. Rocha and L. D. Carlos, *ACS Nano*, 2013, **7**, 7213; b) C. D. S. Brites, P. P. Lima, N. J. O. Silva, A. Millán, V. S. Amaral, F. Palacio and L. D. Carlos, *Adv. Mater.*, 2010, **22**, 4499.
- J. Feng, K. J. Tian, D.H. Hu, S. Q. Wang, S. Y. Li, Y. Zeng, Y. Li, and G. Q. Yang, *Angew. Chem. Int. Ed.*, 2011, **50**, 8072.
- a) F. Wang and X. G. Liu, *Chem. Soc. Rev.*, 2009, **38**, 976; b) R. Weissleder, *Nat. Biotechnol.*, 2001, **19**, 316.
- F. Vetrone, R. Naccache, A. Zamarrón, A. Juarranz de la Fuente, F. Sanz-Rodríguez, L. M. Maestro, E. M. Rodriguez, D. Jaque, J. G. Solé and J. A. Capobianco, *ACS Nano*, 2010, **4**, 3254.
- N.-N. Dong, M. Pedroni, F. Piccinelli, G. Conti, A. Sbarbati, J. E. Ramírez-Hernández, L. M. Maestro, M. C. Iglesias-de la Cruz, F. Sanz-Rodríguez, A. Juarranz, F. Chen, F. Vetrone, J. A. C. G. Solé, M. Bettinelli, D. Jaque and A. Speghini, *ACS Nano*, 2011, **5**, 8665.
- D. Wawrzynczyk, A. Bednarkiewicz, M. Nyk, W. Strek and M. Samoc, *Nanoscale*, 2012, **4**, 6959.
- a) Y. J. Cui, H. Xu, Y. F. Yue, Z. Y. Guo, J. C. Yu, Z. X. Chen, J. K. Gao, Y. Yang, G. D. Qian and B. L. Chen, *J. Am. Chem. Soc.*, 2012, **134**, 3979; b) X. T. Rao, T. Song, J. K. Gao, Y. J. Cui, Y. Yang, C. D. Wu, B. L. Chen and G. D. Qian, *J. Am. Chem. Soc.*, 2013, **135**, 15559.
- a) Y. S. Liu, D. T. Tu, H. M. Zhu and X. Y. Chen, *Chem. Soc. Rev.*, 2013, **42**, 6924; b) L. H. Fischer, G. S. Harms and O. S. Wolfbeis, *Angew. Chem. Int. Ed.*, 2011, **50**, 4546.
- a) Y.-F. Wang, G.-Y. Liu, L.-D. Sun, J.-W. Xiao, J.-C. Zhou and C.-H. Yan, *ACS Nano*, 2013, **7**, 7200; b) X. J. Xie, N. Y. Gao, R. R. Deng, Q. Sun, Q.-H. Xu and X. G. Liu, *J. Am. Chem. Soc.*, 2013, **135**, 12608; c) H. L. Wen, H. Zhu, X. Chen, T. F. Huang, B. L. Wang, G. Y. Zhu, S. F. Yu and F. Wang, *Angew. Chem. Int. Ed.*, 2013, **52**, 13419.
- a) F. Wang, J. Wang and X. G. Liu, *Angew. Chem. Int. Ed.*, 2010, **49**, 7456; b) F. Wang, R. R. Deng, J. Wang, Q. X. Wang, Y. Han, H. M. Zhu, X. Y. Chen and X. G. Liu, *Nat. Mater.*, 2011, **10**, 968; c) Q. Q. Su, S. Y. Han, X. J. Xie, H. M. Zhu, H. Y. Chen, C.-K. Chen, R.-S.

- Liu, X. Y. Chen, F. Wang and X. G. Liu, *J. Am. Chem. Soc.*, 2012, **134**, 20849.
- 12 a) R. T. Wegh, H. Donker, K. D. Oskam and A. Meijerink, *Science*, 1999, **283**, 663; b) D. Y. Wang, N. Kodama, L. Zhao and Y. H. Wang, *J. Electrochem. Soc.*, 2010, **157**, J233.
- 13 Y. S. Liu, D. T. Tu, H. M. Zhu, R. F. Li, W. Q. Luo and X. Y. Chen, *Adv. Mater.*, 2010, **22**, 3266.
- 14 a) C. D. S. Brites, P. P. Lima, N. J. O. Silva, A. Millán, V. S. Amaral, F. Palacio and L. D. Carlos, *New J. Chem.*, 2011, **35**, 1177; b) V. K. Rai, *Appl. Phys. B*, 2007, **88**, 297.
- 15 G. F. Imbusch and B. Henderson, *Optical Spectroscopy of Inorganic Solids*, Oxford Science Publication, London, 2006.
- 16 a) L. D. Carlos, R. A. SáFerreira, J. P. Rainho and V. de Zea Bermudez, *Adv. Funct. Mater.*, 2002, **12**, 819; b) A. Shalav, B. S. Richards and M. A. Green, *Solar Energy Materials & Solar Cell*, 2007, **91**, 829.
- 17 R. Martín-Rodríguez, S. Fischer, A. Ivaturi, B. Froehlich, K. W. Krämer, J. C. Goldschmidt, B. S. Richards and A. Meijerink, *Chem. Mater.*, 2013, **25**, 1912.